Luminescence polarization of silicon nanocrystals

G. Allan,* C. Delerue, and Y. M. Niquet
Institut d'Electronique et de Microélectronique du Nord Département Institut Supérieur d'Electronique du Nord 41 boulevard Vauban, 59046 Lille Cédex, France

(Received 18 January 2000; revised manuscript received 10 October 2000; published 12 April 2001)

We consider theoretically the polarization of the luminescence of Si nanocrystals that arises from the anisotropy of the optical moments. No-phonon and phonon-assisted optical transitions are calculated in tight binding and interpreted using effective-mass theory. In contrast to direct-gap semiconductors, we show that simple selection rules cannot be established in Si nanocrystals because the degree of linear polarization presents large oscillations with respect to the size of the clusters. This effect is due to the indirect nature of the Si band gap that leads to a dependence of the optical matrix elements on the oscillatory overlaps between electron and hole states in momentum space. However, in a statistical ensemble of crystallites elongated in a given direction and with size larger than 2–3 nm, we obtain that the light is in average polarized along this direction, in agreement with the experiments.

DOI: 10.1103/PhysRevB.63.205301 PACS number(s): 78.55.Mb, 73.22.−f

I. INTRODUCTION

The investigation of low-dimensional semiconductor structures has attracted much attention in recent years. In particular, the spectroscopy of optical transitions across the band gap has proved to be a powerful method to study their electronic states. In asymmetric structures, the optical transitions have often a strong dependence on the light polarization. This effect has been extensively studied in III–V heterostructures such as quantum wells[1] or wires[2–4] and in II–VI nanocrystals.[5,6] All these studies concern direct-gap semiconductors where the polarization anisotropy mainly results from two independent factors. The first one comes from the anisotropy of transition dipole moments and the second one arises from a difference between the dielectric constant of the semiconductor and its surrounding medium (the so-called dielectric model). On the theoretical side, the prediction of anisotropic dipole moments is usually based on the framework of the effective-mass approximation[1,4,6] (EMA) that provides simple interpretations of the optical selection rules. The situation is not so clear in indirect-gap semiconductors like silicon. Studies of the optical properties of silicon nanostructures have been stimulated by the discovery of the strong luminescence of porous silicon[7] that is sometimes characterized by a huge degree of linear polarization (up to 30%).[8–12] An interpretation of these experiments has been proposed on the basis of the dielectric model[9,10] where porous silicon is described by ellipsoidal Si crystals embedded in an effective dielectric medium with a lower dielectric constant. The polarization anisotropy that results from the dipole moments is not considered in these models. Actually, the degree of polarization coming from this effect is not known, as a corresponding theory is missing. More generally, the selection rules applicable to optical transitions in anisotropic nanocrystals of indirect-gap semiconductors have not been established in contrast to direct-gap ones. In silicon, one complication arises from the fact that phonon-assisted transitions are more efficient than no-phonon ones in a wide range of nanocrystal sizes.[13,14] The aim of this paper is to study theoretically the anisotropy of the optical transitions in asymmetric silicon nanocrystals. We present detailed tight-binding calculations on clusters with various shapes and sizes. We show that, in contrast to direct-gap semiconductors, the polarization anisotropy is extremely sensitive to the boundary conditions, i.e., the surface of the quantum structure. A consequence is that the degree of linear polarization can vary completely between two crystallites with very close shapes. We also show that, for a statistical distribution of nanocrystals with elongated shapes oriented in a given direction, the luminescence should be polarized in average along this direction. We provide simple interpretations of the tight-binding results using EMA.

The paper is organized as follows. We first describe the tight-binding technique used to calculate the recombination rates for no-phonon and phonon-assisted transitions. In Sec. III, we present the results for no-phonon transitions that we interpret using a method of projection of the confined electron and hole states in momentum space. In Sec. IV, we analyze these results using EMA calculations. In Sec. V, we show that the results for phonon-assisted transitions are close to the no-phonon case and we compare the results to the experiments.

II. TIGHT-BINDING CALCULATIONS

The first step of our paper is the calculation of the electron and hole states of silicon nanocrystals. We use a tight-binding technique with a minimal basis set of one *s* and three *p* orbitals on each silicon atom. The Hamiltonian includes interactions up to third-nearest neighbors and three center terms. Their parametrization, described in Ref. 15, allows one to get a very good silicon band structure that is a necessary condition to obtain correct predictions of the confinement energies.[16] The surfaces of such nanostructures are passivated by hydrogen atoms as in Ref. 17.

The second step of our paper is the calculation of the optical transition rates with respect to the polarization of the light. We first consider the direct recombination of electron-hole pairs, i.e., no-phonon processes. The radiative recombination rate is defined from the dipole matrix elements[18]

$$W_{if}(\mathbf{e}) = AE_{if}|\langle i|\mathbf{e}\cdot\mathbf{p}|f\rangle|^2, \tag{1}$$

where $|i\rangle$ is the initial state of the electron in the conduction band and $|f\rangle$ is the final state in the valence band (i.e., the hole state). E_{if} is the energy of the transition, $\mathbf{e}$ is the vector of the light polarization and A is a constant. The momentum matrix element $\langle i|\mathbf{e}\cdot\mathbf{p}|f\rangle$ is developed in the tight-binding basis where the atomic orbitals are replaced by Gaussians.[19] This method has already been applied to Si (Ref. 20) and CdS (Ref. 21) nanocrystals, and to the isolated dangling bond in silicon.[22] To include the effect of the temperature, we define a thermal average of the recombination rates

$$\langle W(\mathbf{e})\rangle = \frac{\sum_{i,f} W_{if}(\mathbf{e})\exp(-E_{if}/kT)}{\sum_{i,f} \exp(-E_{if}/kT)}. \tag{2}$$

This equation is justified by the fact that the thermalization of the electron and the hole after excitation in the bands is more efficient than the radiative recombination (the radiative recombination rate is smaller than $10^7\ \mathrm{s}^{-1}$ as already shown in Ref. 20). Then we calculate the degree of linear polarization of the emitted light that we define as usual by

$$\sigma = \frac{\langle W(\mathbf{e}_\parallel)\rangle - \langle W(\mathbf{e}_\perp)\rangle}{\langle W(\mathbf{e}_\parallel)\rangle + \langle W(\mathbf{e}_\perp)\rangle}, \tag{3}$$

where $\mathbf{e}_\parallel$ and $\mathbf{e}_\perp$ are two orthogonal vectors ($\mathbf{e}_\parallel$ will be fixed with respect to the longest axis of the nanostructure). It is important to point out that σ calculated here only describes the polarization anisotropy that arises from the anisotropy of the dipole moments. Other factors like dielectric effects—which would make the constant A in Eq. (1) dependent on the polarization vector $\mathbf{e}$—are not considered here since they have already been analyzed in detail in references such as Ref. 9.

To calculate the recombination rates for phonon-assisted transitions, we start again from Eq. (1). But now, the states $|i\rangle$ and $|f\rangle$ include the coordinates of the electron and of the nuclei. Working within the adiabatic approximation, the matrix element of the momentum becomes

$$\langle i|\mathbf{e}\cdot\mathbf{p}|f\rangle = \langle\chi_i|\langle\psi_i|\mathbf{e}\cdot\mathbf{p}|\psi_f\rangle|\chi_f\rangle. \tag{4}$$

$|\chi_i\rangle$ and $|\chi_f\rangle$ are the vibrational states of the system that are functions of the nuclear coordinates. They are built in the harmonic approximation from independent harmonic oscillators corresponding to $3N$ normal modes Q_j (N is the number of atoms in the system). $|\psi_i\rangle$ and $|\psi_f\rangle$ in Eq. (4) are the electronic wave functions that can be defined for any set of nuclear coordinates. We can expand the momentum matrix element to first order in the normal modes

$$\langle\psi_i|\mathbf{p}|\psi_f\rangle = \langle\psi_i|\mathbf{p}|\psi_f\rangle_0 + \sum_{j=1}^{3N} \mathbf{A}_j\langle\chi_i|Q_j|\chi_f\rangle, \tag{5}$$

where $\mathbf{A}_j = (\partial\langle\psi_i\mathbf{p}|\psi_f\rangle/\partial Q_j)_0$. The index 0 means that the quantities are calculated at the equilibrium positions. Using the transformation $Q_j = \sqrt{\hbar/2\omega_j}(a_j^+ + a_j)$ as a function of the creation and annihilation operators and averaging over n_j, the number of phonons in mode j, we obtain the following recombination rates for one-phonon processes after straightforward algebra (details will be given in another publication[23])

$$\text{one-phonon emission } (\hbar\omega_j): W_{if}(\mathbf{e}) \approx K\left|\sqrt{\frac{\hbar}{2\omega_j}}\mathbf{A}_j\cdot\mathbf{e}\right|^2\{\overline{n_j}+1\}, \tag{6}$$

$$\text{one-phonon absorption } (\hbar\omega_j): W_{if}(\mathbf{e}) \approx K\left|\sqrt{\frac{\hbar}{2\omega_j}}\mathbf{A}_j\cdot\mathbf{e}\right|^2\overline{n_j}, \tag{7}$$

where $\overline{n_j} = [\exp(\hbar\omega_j/kT)-1]^{-1}$. The heavy part of the work is the evaluation of the coupling coefficients $\mathbf{A}_j$, which are calculated numerically for all the modes j of the quantum dot. For each mode j, it requires to calculate the wave functions—therefore the Hamiltonian—and the optical matrix elements when the nuclei are displaced from their equilibrium sites according to Q_j. The matrix elements of the Hamiltonian are made dependent on the atomic positions following the rules of Ref. 24. The vibrational modes of the nanocrystals are calculated using a valence force field model.[25] The main results of these calculations will be published elsewhere,[23] as we concentrate here on the polarization. To summarize these results, we confirm that the transitions are mainly assisted by transverse-optic (TO) and longitudinal-optic modes, with smaller contributions from transverse-acoustic (TA) phonons, in agreement with the theoretical work of Ref. 13 and with the experiments.[14,26]

III. TIGHT-BINDING RESULTS FOR NO-PHONON TRANSITIONS

We have mainly studied Si dielectric ellipsoids as they are considered in the microscopic description of porous silicon.[9] The ellipsoids are defined as usual by three principal axes of respective length a, b, c, with a oriented along a [100] axis and $b=c=a/\sqrt{2}$. The polarization degree σ for no-phonon transitions is plotted in Fig. 1 with respect to a ($T=300\ \mathrm{K}$). We see that for $a<2$ nm, σ is scattered and gets positive or negative values, but for larger sizes, σ tends to become positive in average. It is particularly interesting to compare thus with the results obtained for ellipsoids with a similar shape but with a long axis oriented along a [110] direction (dashed lines in Fig. 1). We see that the two curves do not coincide in spite of the great similarity of the nanocrystals. However, in both cases, σ oscillates between positive or negative values for small lengths (<3 nm) and tends to remain positive for bigger crystallites. Similar behavior is obtained for ellipsoids with the long axis a oriented along [100] but with $a=\sqrt{2}b=2c$ (Fig. 2). All these results are rather surprising at first glance and they have no equivalence in the case of direct-gap semiconductors.

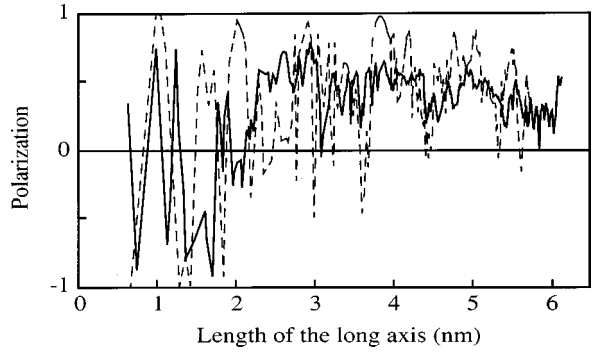

FIG. 1. The polarization degree for Si ellipsoids oriented along a [100] direction (straight line) or a [110] direction (dashed line) calculated as a function of the length of the long axis, which is equal to $\sqrt{2}$ times the length of small ones ($T=300$ K).

In many experiments (for example, the photoluminescence of porous silicon), one must take into account that the samples are heterogeneous. Since there is no *a priori* way for choosing a particular distribution of crystallite sizes and shapes, the problem is inherently complex taking into account the oscillations of σ. However, we have seen in the preceding section that σ becomes positive in average for sizes larger than 2–3 nm. We have checked that this conclusion holds true for other types of asymmetric nanocrystals such as cylinders or boxes (parallelepipeds). Figure 3 shows the degree of linear polarization calculated for boxes bounded by (100) planes and of dimensions $L_\perp, L_\perp, L_\parallel$ in the *x, y, z* directions respectively. σ is defined with respect to the *z* axis ($\mathbf{e}_\parallel=\mathbf{z}$). When $L_\parallel=L_\perp$ (cubic crystallites), σ is equal to zero as imposed by the symmetry. When $L_\parallel>L_\perp$, σ is positive and, when $L_\parallel<L_\perp$, σ is negative, which means that the light is always polarized along the largest dimension. We also note that there are less oscillations than in the case of the ellipsoids (however, the results obtained at 10 K again show large oscillations).

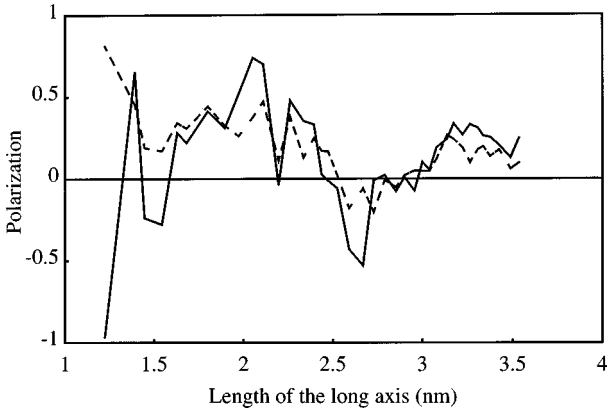

FIG. 2. Polarization degree for Si ellipsoids oriented along a [100] direction calculated as a function of the length of the long axis ($T=300$ K). The [100] ellipsoid axis is equal to $\sqrt{2}$ times the [010] one and to two times the [001] one (straight lines: no-phonon transitions, dashed lines: phonon-assisted transitions).

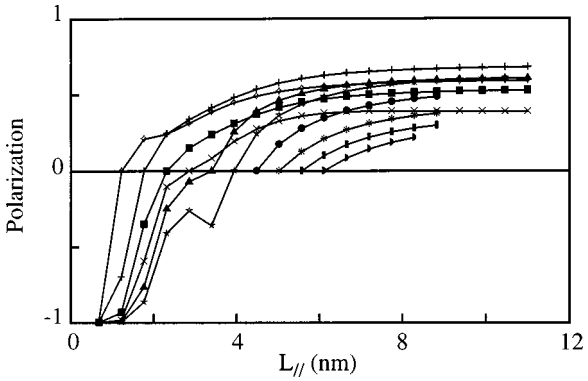

FIG. 3. Polarization degree for $L_\perp \times L_\perp \times L_\parallel$ boxes bounded by (100) planes ($T=300$ K). The results are plotted versus $L_\parallel$ for different values of $L_\perp$: 1.22 nm (✧), 1.76 nm (+), 2.31 nm (■), 2.85 nm (×), 3.39 nm (▲), 3.93 nm (⋆), 4.48 nm (●), 5.02 nm (*), 5.56 nm, (▮), 6.10 nm (◗). The polarization is equal to zero for $L_\perp = L_\parallel$.

IV. INTERPRETATION USING EFFECTIVE-MASS THEORY

To understand the peculiar behavior of the polarization, we analyze in detail the nature of the no-phonon transitions. We come back to important points that have been discussed in detail in Refs. 20, 27. Because of the indirect gap, band-edge transitions in bulk Si are only possible with the assistance of phonons to supply the momentum in a second-order process. In nanocrystals, the strong confinement of the electron and hole wave functions in real space leads to a spread of the wave functions in momentum space. Thus, radiative recombination can proceed by direct no-phonon transitions and the oscillator strength is directly proportional to the reciprocal space overlap. To illustrate this effect, we plot on Fig. 4 the weight of the lowest electron state ψ_e and of the highest hole state ψ_h in momentum space. To obtain these values, we project the tight-binding eigenfunctions in the basis of the bulk states

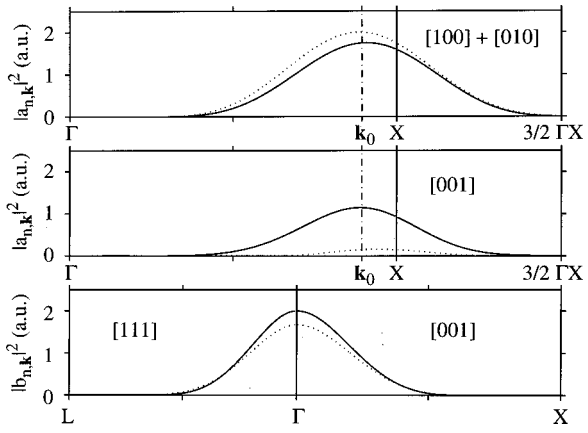

FIG. 4. Top: projection ($|a_{n,\mathbf{k}}|^2$) of the lowest electron state in an ellipsoid on the bulk states $\Psi_{n,\mathbf{k}}$ for $\mathbf{k}$ along [100] and [010] (sum of the two). Middle: same for $\mathbf{k}$ along [001]. Bottom: projection ($|b_{n,\mathbf{k}}|^2$) of the highest hole state for $\mathbf{k}$ along [001] (right) and [111] (left). Solid lines: ellipsoid long axis of 1.90 nm, short axis of 1.36 nm. Dashed line: long axis of 2.17 nm, short axis of 1.36 nm.

$$\psi_e = \sum_{n,\mathbf{k}} a_{n,\mathbf{k}} \Psi_{n,\mathbf{k}},$$

$$\psi_h = \sum_{n,\mathbf{k}} b_{n,\mathbf{k}} \Psi_{n,\mathbf{k}}, \tag{8}$$

where the index n enumerates the bands. The dipole matrix element is given by

$$\langle \psi_e | \mathbf{e}\cdot\mathbf{p} | \psi_h \rangle = \sum_{n,n',\mathbf{k}} a_{n,\mathbf{k}}{}^* b_{n',\mathbf{k}} \langle \Psi_{n,\mathbf{k}} | \mathbf{e}\cdot\mathbf{p} | \Psi_{n',\mathbf{k}} \rangle. \tag{9}$$

Figure 4 shows that the overlap ($a_{n,\mathbf{k}}{}^* b_{n',\mathbf{k}}$) of ψ_e and ψ_h in momentum space is small because ψ_e is centered at the conduction-band minima ($\mathbf{k}=\mathbf{k}_0$) and ψ_h is centered at $\mathbf{k}=0$. It explains why the radiative lifetime remains long in silicon crystallites.[20,27] As $a_{n,\mathbf{k}}$ and $b_{n',\mathbf{k}}$ are oscillatory functions of $\mathbf{k}$ (Fig. 4 and below), oscillatory factors enter the optical matrix elements and the degree of polarization. An additional source of scattering comes from the fact that $\langle \Psi_{n,\mathbf{k}} | \mathbf{e}\cdot\mathbf{p} | \Psi_{n',\mathbf{k}} \rangle$ is not a constant with respect to $\mathbf{k}$.

To understand the origin of the average linear polarization of the no-phonon transitions along the long axis of the nanostructures, we use the EMA, following closely Ref. 27. Even if the EMA has been designed to treat shallow potentials in semiconductors, its application to semiconductor heterostructures and nanostructures is now widely developed.[1] The advantage of the EMA is its simplicity that allows us to get analytic results. However, its accuracy (e.g., for the band-gap energy) is not sufficient in many situations, in particular compared to more elaborate techniques like tight binding (see the discussion in Ref. 28). We consider a box of volume $L_\perp L_\perp L_\parallel$. Under the assumption of an infinite barrier at the boundary of the crystallite, the envelope function for electrons and holes is

$$F(\mathbf{r}) = \sqrt{\frac{8}{L_\perp^2 L_\parallel}} \cos\left(\frac{\pi x}{L_\perp}\right) \cos\left(\frac{\pi y}{L_\perp}\right) \cos\left(\frac{\pi z}{L_\parallel}\right)$$

$$\text{with} \quad \begin{matrix} -L_\perp/2 \leqslant x,y \leqslant L_\perp/2 \\ -L_\parallel/2 \leqslant z \leqslant L_\parallel/2 \end{matrix}. \tag{10}$$

One difficulty in the problem is that there are six equivalent (100) electron valleys in the Si conduction band (denoted x, $\overline{x}$, y, $\overline{y}$, z, $\overline{z}$, in the following). We assume for the moment that the treatment of the six minima can be decoupled. Because these valleys are anisotropic with a longitudinal mass $m_l = 0.92 m_0$ and a transverse mass $m_t = 0.19 m_0$, the confinement energies are (in atomic units)

$$\Delta E = \frac{1}{2m_l}\left(\frac{\pi}{L_\parallel}\right)^2 + \frac{1}{m_t}\left(\frac{\pi}{L_\perp}\right)^2, \tag{11}$$

for states arising from z and $\overline{z}$ valleys and

$$\Delta E = \frac{1}{2m_l}\left(\frac{\pi}{L_\perp}\right)^2 + \frac{1}{2m_t}\left[\left(\frac{\pi}{L_\perp}\right)^2 + \left(\frac{\pi}{L_\parallel}\right)^2\right], \tag{12}$$

for x, $\overline{x}$, y, $\overline{y}$. In the case of a box with $L_\parallel > L_\perp$, the lowest electron states arise from the four equivalent minima [Eq. (12)]. Following Eqs. (8) and (9), the evaluation of the dipole matrix elements requires us to write the total wave function in the basis of the bulk states $\Psi_{n,\mathbf{k}}$. Since the coupling between the different bands is neglected (in particular, between the conduction band valleys), the sum in Eq. (8) is restricted to the highest valence band $\Psi_{\nu,\mathbf{k}}$ for the hole state ψ_h and to the lowest conduction bands $\Psi_{jc,\mathbf{k}}$ for an electron state ψ_{je} (j enumerates the four equivalent minima). Following standard EMA (Refs. 27, 29), we obtain

$$\psi_h = \sum_{\mathbf{k}} F(\mathbf{k}) \Psi_{\nu,\mathbf{k}},$$

$$\psi_{je} = \sum_{\mathbf{k}} F(\mathbf{k}-\mathbf{k}_{0j}) \Psi_{jc,\mathbf{k}}, \tag{13}$$

where $F(\mathbf{k})$ is the Fourier transform of the envelope function and $\mathbf{k}_{0j}$ is the wave vector at the conduction-band minimum j. Thus, the dipole matrix element [Eq. (9)] is given by

$$\langle \psi_{je} | \mathbf{e}\cdot\mathbf{p} | \psi_h \rangle = \sum_{\mathbf{k}} F(\mathbf{k}-\mathbf{k}_{0j})^* F(\mathbf{k}) \langle \Psi_{jc,\mathbf{k}} | \mathbf{e}\cdot\mathbf{p} | \Psi_{\nu,\mathbf{k}} \rangle. \tag{14}$$

We need to calculate this matrix element for two polarizations $\mathbf{e}_\parallel = z$ and $\mathbf{e}_\perp = \mathbf{x}$. Let us consider specifically the electron state ψ_{xe} corresponding to the x valley [$\mathbf{k}_{0x} \approx 0.89(2\pi/a)\mathbf{x}$]. Since $F(\mathbf{k})$ and $F(\mathbf{k}-\mathbf{k}_{0x})$ are centered at $\mathbf{k}=0$ and $\mathbf{k}=\mathbf{k}_{0x}$, respectively, we expect that the maximum of their overlap [$F(\mathbf{k}-\mathbf{k}_{0x})^* F(\mathbf{k})$] is in the vicinity of the [100] axis of the momentum space. Thus, we have analyzed the optical matrix element $\langle \Psi_{xc,\mathbf{k}} | \mathbf{e}\cdot\mathbf{p} | \Psi_{\nu,\mathbf{k}} \rangle$ in this region using the tight-binding wave functions of bulk silicon. We obtain that for x polarization, the matrix element is equal to zero along the [100] axis. For z polarization, it is not equal to zero and we will assume that it is approximately independent of $\mathbf{k}$.[30] Therefore, in the vicinity of the [100] axis, we can write to the first significative order

$$\langle \Psi_{xc,\mathbf{k}} | p_x | \Psi_{\nu,\mathbf{k}} \rangle \approx \alpha(k_y + k_z),$$

$$\langle \Psi_{xc,\mathbf{k}} | p_z | \Psi_{\nu,\mathbf{k}} \rangle \approx \beta, \tag{15}$$

where α and β are two complex scalars. Inserting Eq. (15) into Eq. (14), we obtain

$$\langle \psi_{xe} | p_x | \psi_h \rangle = \alpha \sum_{\mathbf{k}} F(\mathbf{k}-\mathbf{k}_{0x})^* F(\mathbf{k}) (k_y + k_z) = 0,$$

$$\langle \psi_{xe} | p_z | \psi_h \rangle = \beta \sum_{\mathbf{k}} F(\mathbf{k}-\mathbf{k}_{0x})^* F(\mathbf{k})$$

$$= \beta \int e^{i\mathbf{k}_{0x}\cdot\mathbf{r}} |F(\mathbf{r})|^2 d\mathbf{r}, \tag{16}$$

$\langle \psi_{xe} | p_x | \psi_h \rangle$ is equal to zero because $F(\mathbf{k}-\mathbf{k}_{0x})$ and $F(\mathbf{k})$ are invariant when one changes k_y into $-k_y$ due to the sym-

metry of the envelope function. The same result is obtained for the electron states arising from the $\overline{x}$ valley. For the y valley [$\mathbf{k}_{0y} \approx 0.89(2\pi/a)\mathbf{y}$], the same analysis leads to

$$\langle \psi_{ye}|p_x|\psi_h\rangle = \langle \psi_{ye}|p_z|\psi_h\rangle = \beta \int e^{i\mathbf{k}_{0y}\cdot\mathbf{r}}|F(\mathbf{r})|^2 d\mathbf{r}, \tag{17}$$

and to identical results for $\psi_{\overline{y}e}$. The integrals in Eqs. (16) and (17) are equal by symmetry[27]

$$\begin{aligned} &\int e^{i\mathbf{k}_{0j}\cdot\mathbf{r}}|F(\mathbf{r})|^2 d\mathbf{r} \\ &\quad = M(L_\perp) \\ &\quad = -\frac{1}{\pi k_{0j}}\left(\frac{2\pi}{L_\perp}\right)^3 \left[k_{0j}^2 - \left(\frac{2\pi}{L_\perp}\right)^2\right]^{-1} \sin\left(\frac{k_{0j}L_\perp}{2}\right), \end{aligned} \tag{18}$$

for $j = x, \overline{x}, y, \overline{y}$. Then, we calculate the total recombination rate for x and z polarizations using Eq. (1)

$$\begin{aligned} \langle W(\mathbf{x})\rangle &= AE_0 \sum_j |\langle \psi_{je}|p_x|\psi_h\rangle|^2 = 2AE_0\beta^2 M(L_\perp)^2, \\ \langle W(z)\rangle &= AE_0 \sum_j |\langle \psi_{je}|p_z|\psi_h\rangle|^2 = 4AE_0\beta^2 M(L_\perp)^2, \end{aligned} \tag{19}$$

where $j \in \{x, \overline{x}, y, \overline{y}\}$. The degree of linear polarization is equal to

$$\sigma = \frac{\langle W(z)\rangle - \langle W(\mathbf{x})\rangle}{\langle W(z)\rangle + \langle W(\mathbf{x})\rangle} \rightarrow \frac{1}{3} \quad \text{when} \quad M(L_\perp) \neq 0. \tag{20}$$

The oscillatory function $M(L_\perp)$ simplifies because it factorizes both in the numerator and in the denominator. It is then straightforward to calculate σ in the case of a box with $L_\parallel < L_\perp$. The lowest electron states arise from z and $\overline{z}$ valleys. The optical matrix elements are

$$\begin{aligned} \langle \psi_{ze}|p_x|\psi_h\rangle &= \beta \int e^{i\mathbf{k}_{0z}\cdot\mathbf{r}}|F(\mathbf{r})|^2 d\mathbf{r} = \beta M(L_\parallel), \\ \langle \psi_{ze}|p_z|\psi_h\rangle &= 0, \end{aligned} \tag{21}$$

with similar results for $\psi_{\overline{z}e}$. The recombination rates become

$$\begin{aligned} \langle W(\mathbf{x})\rangle &= 2AE_0\beta^2 M(L_\parallel)^2, \\ \langle W(z)\rangle &= 0, \end{aligned} \tag{22}$$

which gives, for the degree of polarization

$$\sigma \rightarrow -1 \quad \text{when} \quad M(L_\parallel) \neq 0. \tag{23}$$

Thus, this simple EMA model qualitatively explains the tight-binding results of Fig. 3 where $\sigma > 0$ when $L_\parallel > L_\perp$ and $\sigma \approx -1$ when $L_\parallel < L_\perp$. However, when $L_\parallel > L_\perp$, the tight-binding calculations predict a value of σ, which differs from 1/3 and depends on $L_\perp$ (it is independent of $L_\parallel$, when $L_\parallel \gg L_\perp$). The origins of this dependence are twofold: (i) the coupling between $x, \overline{x}, y, \overline{y}$ valleys that leads to a splitting of the four degenerate states; (ii) the electron and hole states have nonzero projections on all valence and conduction bands. We discuss these effects in the Appendix.

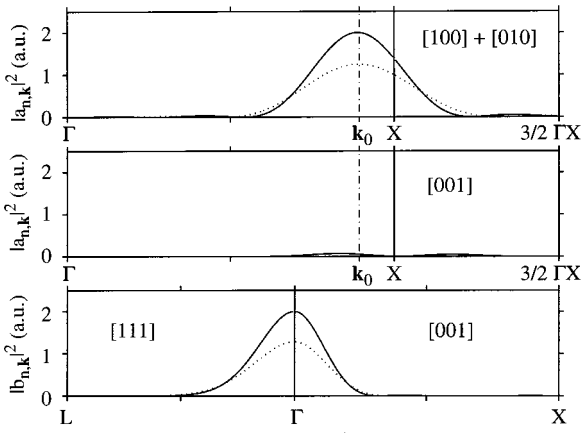

FIG. 5. Top: projection ($|a_{n,\mathbf{k}}|^2$) of the lowest electron state in a $L_\perp \times L_\perp \times L_\parallel$ box on the bulk states $\Psi_{n,\mathbf{k}}$ for $\mathbf{k}$ along [100] and [010] (sum of the two). Middle: same for $\mathbf{k}$ along [001]. Bottom: projection ($|b_{n,\mathbf{k}}|^2$) of the highest hole state for $\mathbf{k}$ along [001] (right) and [111] (left). Solid lines: $L_\parallel = 1.90$ nm, $L_\perp = 1.36$ nm. Dashed line: $L_\parallel = 2.17$ nm, $L_\perp = 1.63$ nm.

The mixing of the states arising from $x, \overline{x}, y, \overline{y}$ valleys is confirmed by the analysis of the tight-binding wave functions that shows, in addition, that the coupling to z and $\overline{z}$ valleys is weak in the case of boxes (Fig. 5). In the case of the elongated ellipsoids discussed in the preceding section, the coupling to z and $\overline{z}$ is stronger (Fig. 4), in particular in small nanostructures. The main consequence is that the optical matrix elements between electron and hole states include combinations of terms like $M(L_\perp)$ and $M(L_\parallel)$ which are oscillatory functions [Eq. (18)]. As these functions do not simplify in the expression of σ [Eq. (20)], it leads to strong oscillations for ellipsoids (the intervalley couplings also contribute to the oscillations; see Appendix). However, for the largest ones, because the lower electron states mainly arise from $x, \overline{x}, y, \overline{y}$ valleys, the contribution of $M(L_\parallel)$ becomes smaller, which explains the positive value of σ in average.

An important point to consider is the accuracy of our tight-binding predictions. In particular, we need to discuss effects beyond one-particle approximations such as the electron-hole interaction in the excited state. Thus, we have performed calculations of σ taking into account excitonic effects. Following the procedure of Refs. 17 and 21, the exciton wave function is written as a linear combination of Slater determinants built from one-electron states and corresponding to single electron-hole excitations. The Hamiltonian includes the screened electron-hole Coulomb interaction, exchange interactions and spin-orbit coupling. Details on the calculation can be found in Refs. 17 and 21. Applied to elongated ellipsoids, we obtain results qualitatively very close to those of single-particle calculations with many os-

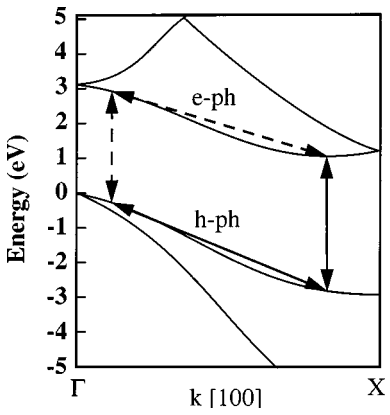

FIG. 6. The Si band structure near the gap region along the (100) direction. The processes for phonon-assisted transitions are illustrated.

cillations for small sizes and a positive value in average for larger sizes. This result is not surprising, because in the strong confinement regime, the main effect of the electron-hole interaction in confined systems is just to shift downward the transition energy and to split states arising from the same multiplet (equivalent valleys). Another point to consider is the importance of phonon-assisted transitions that remain more efficient than no-phonon ones.[13] We analyze these processes in the next section.

V. PHONON-ASSISTED TRANSITIONS

We consider for example the ellipsoids with a long axis a oriented along [100] and with $a=\sqrt{2}b=2c$ (Fig. 2). Comparing no-phonon and phonon-assisted transitions, we see that the behavior of σ is quite similar. In particular, σ tends to become positive at large sizes and the oscillations at small sizes are correlated. To understand why σ tends to become positive in average, we can use the qualitative picture of Fig. 6. The electron-hole transition involves an electron- or hole-phonon scattering event. Thus, the vertical optical transition occurs, either near a conduction-band minimum $\mathbf{k}=\mathbf{k}_0$, or near $\mathbf{k}=0$. In the first case ($\mathbf{k}=\mathbf{k}_0$), the discussion of the preceding section about the polarization of no-phonon transitions in the vicinity of [100] axes can be used here, leading to the same conclusion. In the second case ($\mathbf{k}=0$), we recover the situation of a direct-gap material, where the optical dipole moments are polarized along the long axis of a nanostructure.[4,6] Therefore, the two channels for the transition lead to a positive degree of polarization. The oscillations of σ at small sizes arise from the intervalley couplings that are oscillatory functions of the size (Appendix). The oscillations for no-phonon and phonon-assisted transitions are correlated because they both depend on the decomposition of the electron wave function in the six valleys of the conduction band.

Thus, our calculations predict an average positive polarization degree, in agreement with many experiments on porous silicon or on silicon nanocrystals.[8–12] However, as mentioned in the introduction, a large part of the polarization degree may be explained by dielectric effects due to the fact that the silicon nanocrystals are embedded in an effective medium with a lower dielectric constant.[9,10] However, recent photoluminescence experiments on porous silicon show that the positive polarization degree is larger under resonant excitation than under nonresonant conditions.[31] This is interpreted by the authors by a polarization of the dipole moment in anisotropic nanocrystals, which is totally supported by our calculations. In addition, the photoluminescence observed under resonant excitation shows onsets related to no-phonon, TO, and TA phonon-assisted transitions. The enhancement of the polarization degree compared to the nonresonant spectrum is obtained in the three cases, once again in agreement with our results.

In conclusion, we have performed tight-binding calculations of the degree of linear polarization σ in asymmetric silicon nanocrystals. σ presents large oscillations with respect to the size of the clusters. This effect, which has no counterpart in the case of direct-gap semiconductors, is attributed to the valley degeneracy induced by the indirect nature of the silicon band gap. We also show that for an ensemble of crystallites elongated in a same direction, the light should be preferentially polarized along this direction. Simple effective mass theory is used to interpret this effect. The results are in agreement with the experiments on porous silicon and silicon nanocrystals.

ACKNOWLEDGMENTS

We thank M. V. Wolkin and P. M. Fauchet for helpful discussions. The Institut d'Electronique et de Microélectronique du Nord is UMR 8520 of CNRS.

APPENDIX

In a $L_\perp \times L_\perp \times L_\parallel$ box bounded by (100) planes with $L_\parallel > L_\perp$, the lowest electron states (denoted $\psi_{xe}, \psi_{\overline{xe}}, \psi_{ye}, \psi_{\overline{ye}}$) are associated with the four conduction valleys $x, \overline{x}, y, \overline{y}$. This valley degeneracy predicted in EMA is lifted in actual systems, giving rise to the so-called valley splittings observed in Si inversion layers.[32] An examination of the tight-binding results shows that the couplings between states are not constant but are oscillatory functions of size and are strongly dependent on the boundary conditions.[28] This effect can be roughly understood using EMA wave functions. The coupling between two states ψ_{je} and $\psi_{j'e}(j' \neq j)$ is given by

$$\langle \psi_{je}|H|\psi_{j'e}\rangle = \sum_{\mathbf{k},\mathbf{k}'} F(\mathbf{k}-\mathbf{k}_{0j})^* F(\mathbf{k}'-\mathbf{k}_{0j'}) \times \langle \Psi_{jc,\mathbf{k}}|H|\Psi_{j'c,\mathbf{k}'}\rangle, \quad \text{(A1)}$$

where H is the Hamiltonian of the nanocrystal. Writing $H = H_{\text{bulk}} + U$ where H_{bulk} is the bulk Hamiltonian and U is the confining potential, we obtain

$$\langle \psi_{je}|H|\psi_{j'e}\rangle = \sum_{\mathbf{k},\mathbf{k}'} F(\mathbf{k}-\mathbf{k}_{0j})^* F(\mathbf{k}'-\mathbf{k}_{0j'}) \times \langle \Psi_{jc,\mathbf{k}}|U|\Psi_{j'c,\mathbf{k}'}\rangle. \quad \text{(A2)}$$

The matrix element of U gives rise to interference effects between Bloch states at the surface (a similar term is discussed in Ref. 33). By comparison to Eqs. (16)–(18), and since $\mathbf{k}_{0j} \neq \mathbf{k}_{0j'}$, we are easily convinced that $\langle \psi_{je}|H|\psi_{j'e}\rangle$ is an oscillatory function of the size (a decreasing function because U takes a nonzero value only in the vicinity of the surface). It is clear that a quantitative treatment of these terms cannot be done using EMA since it depends on the surface. However, the symmetry of the system requires that the coupling matrix between the four states has the following form

$$\begin{bmatrix} 0 & \gamma & \delta & \delta \\ \gamma & 0 & \delta & \delta \\ \delta & \delta & 0 & \gamma \\ \delta & \delta & \gamma & 0 \end{bmatrix}, \tag{A3}$$

where γ and δ are functions of $L_\perp, L_\parallel$ and of the boundary conditions. The corresponding eigenvalues and eigenvectors are

$$E_1 = -\gamma, \text{ twofold degenerate, } \frac{\psi_{xe} - \psi_{\overline{x}e}}{\sqrt{2}} \text{ and } \frac{\psi_{ye} - \psi_{\overline{y}e}}{\sqrt{2}}, \tag{A4}$$

$$E_2 = \gamma - 2\delta, \frac{(\psi_{xe} + \psi_{\overline{x}e}) - (\psi_{ye} + \psi_{\overline{y}e})}{2}, \tag{A5}$$

$$E_3 = \gamma + 2\delta, \frac{(\psi_{xe} + \psi_{\overline{x}e}) + (\psi_{ye} + \psi_{\overline{y}e})}{2}. \tag{A6}$$

Let us already notice that the order of E_1 and of E_2 and E_3 changes from one crystallite to another. The probabilities of transition are easily derived from Eqs. (16)–(18), respectively, for the three levels

$$W_1(\mathbf{x}) = W_1(\mathbf{z}) = 0,$$

$$W_2(\mathbf{x}) = AE_0\beta^2 M(L_\perp)^2 \quad W_2(z) = 0,$$

$$W_3(\mathbf{x}) = AE_0\beta^2 M(L_\perp)^2 \quad W_3(\mathbf{z}) = 4AE_0\beta^2 M(L_\perp)^2. \tag{A7}$$

Then we calculate the total recombination rates in terms of the occupation numbers f_1, f_2, f_3 of the orbitals, neglecting states higher in energy (i.e., $2\ f_1 + f_2 + f_3 \approx 1$)

$$\langle W(\mathbf{x})\rangle = (f_2 + f_3)AE_0\beta^2 M(L_\perp)^2,$$

$$\langle W(z)\rangle = 4f_3 AE_0\beta^2 M(L_\perp)^2, \tag{A8}$$

which gives for the degree of polarization

$$\sigma \to \frac{3f_3 - f_2}{5f_3 + f_2} \text{ when } M(L_\perp) \neq 0. \tag{A9}$$

At low temperature, because the respective position of the three levels quickly changes from one crystallite to another and because only the lowest state is populated, σ can take positive or negative values as confirmed by the tight binding calculations. For example, $f_3 = 1, f_2 = 0$ gives $\sigma = 3/5$, while $f_3 = 0, f_2 = 1$ gives $\sigma = -1$. When the temperature increases and the occupancy of the levels becomes uniform ($f_i \approx 1/4$), we recover the preceding result that σ tends towards 1/3. The situation of Fig. 3 is actually intermediate between these two extremes as σ remains positive for $L_\parallel > L_\perp$ but differs from 1/3. When $L_\parallel \gg L_\perp$, the splitting between the three levels becomes independent on $L_\parallel$, which explains the saturation of σ with respect to $L_\parallel$ on Fig. 3. Thus, EMA calculations explain qualitatively the tight-binding results. However, it remains rather crude as shown by the analysis of the tight-binding wave functions (Figs. 4 and 5). The electron states have also a small component on the Bloch states arising from z and $\overline{z}$ valleys. More generally, confined electron and hole states have nonzero projections on all the bands[28] that lead to nonnegligible terms in the optical matrix elements. Obviously, these effects cannot be described in EMA.

*Email address: Guy.Allan@isen.iemn.univ-lille1.fr

[1] G. Bastard, *Wave Mechanics Applied to Semiconductor Heterostructures* (Les Editions de Physique, Les Ulis, France, 1988).

[2] M. Tsuchiya, J. M. Gaines, R. H. Yan, R. J. Simes, P. O. Holtz, L. A. Coldren, and P. M. Petroff, Phys. Rev. Lett. **62**, 466 (1989).

[3] M. Kohl, D. Heitmann, P. Grambow, and K. Ploog, Phys. Rev. Lett. **63**, 2124 (1989).

[4] U. Bockelmann and G. Bastard, Phys. Rev. B **45**, 1688 (1992).

[5] M. G. Bawendi, W. L. Wilson, L. Rothberg, P. J. Carroll, T. M. Jeddju, M. L. Stegerwald, and L. E. Brus, Phys. Rev. Lett. **65**, 1623 (1990).

[6] Al. L. Efros, Phys. Rev. B **46**, 7448 (1992).

[7] L. T. Canham, Appl. Phys. Lett. **57**, 1046 (1990).

[8] A. V. Andrianov, D. I. Kovalev, N. N. Zinov'ev, and I. D. Yaroshetskii, Pis'ma Zh. Eksp. Teor. Fiz. **58**, 417 (1993) [JETP Lett. **58**, 427 (1993)].

[9] D. Kovalev, M. Ben Chorin, J. Diener, F. Koch, Al. L. Efros, M. Rosen, N. A. Gippius, and S. G. Tikhodeev, Appl. Phys. Lett. **67**, 1585 (1995).

[10] P. Lavallard and P. A. Suris, Solid State Commun. **25**, 267 (1995).

[11] W. H. Zheng, J.-B. Xia, and K. W. Cheah, J. Phys.: Condens. Matter **9**, 5105 (1997).

[12] M. V. Wolkin and P. Fauchet (unpublished).

[13] M. S. Hybertsen, Phys. Rev. Lett. **72**, 1514 (1994).

[14] D. Kovalev, H. Heckler, M. Ben-Chorin, G. Polisski, M. Schwartzkopff, and F. Koch, Phys. Rev. Lett. **81**, 2803 (1998).

[15] C. Tserbak, H. M. Polatoglou, and G. Theodorou, Phys. Rev. B **47**, 7104 (1993).

[16] C. Delerue, G. Allan, and M. Lannoo, Phys. Rev. Lett. **76**, 2961 (1996).

[17] E. Martin, C. Delerue, G. Allan, and M. Lannoo, Phys. Rev. B **50**, 18258 (1994).

[18] D. L. Dexter, in *Solid State Physics, Advances in Research and Applications*, edited by F. Seitz and D. Turnbull (Academic, New York, 1958), Vol. 6, p. 360.

[19] J. Petit, G. Allan, and M. Lannoo, Phys. Rev. B **33**, 8595 (1986).

[20] C. Delerue, G. Allan, and M. Lannoo, Phys. Rev. B **48**, 11 024 (1993).

[21] M. Chamarro, M. Dib, V. Voliotis, A. Filoramo, P. Roussignol, T. Gacoin, J. P. Boilot, C. Delerue, G. Allan, and M. Lannoo, Phys. Rev. B **57**, 3729 (1998).
[22] J. Petit, M. Lannoo, and G. Allan, Solid State Commun. **60**, 861 (1986).
[23] C. Delerue, G. Allan, and M. Lannoo (unpublished).
[24] W. A. Harrison, *Electronic Structure and the Properties of Solids* (Freeman, San Francisco, 1980).
[25] R. Tubino, L. Piseri, and G. Zerbi, J. Chem. Phys. **56**, 1022 (1972); D. Vanderbilt, S. H. Taole, and S. Narasimham, Phys. Rev. B **40**, 5657 (1989).
[26] P. D. J. Calcott, K. J. Nash, L. T. Canham, M. J. Kane, and D. Brumhead, J. Phys.: Condens. Matter **5**, L91 (1993).
[27] M. S. Hybertsen, in *Light Emission from Silicon*, edited by S. S. Iyer, L. T. Canham, and R. T. Collins, Mater. Res. Soc. Symp. Proc. No. **256** (Materials Research Society, Pittsburgh, 1992), p. 179.
[28] Y. M. Niquet, C. Delerue, G. Allan, and M. Lannoo, Phys. Rev. B **62**, 5109 (2000).
[29] M. Lannoo and J. Bourgoin, *Point Defects in Semiconductors I. Theoretical Aspects*, Solid State Sciences Vol. 22 (Springer, Berlin, 1981), Chap. 2.
[30] The variations of the p_z matrix element with **k** are small in the region where the reciprocal space overlap is maximum: β can be seen as an average value.
[31] D. Kovalev, H. Heckler, G. Polisski, and F. Koch, Phys. Status Solidi B **215**, 871 (1999).
[32] T. Ando, A. B. Fowler, and F. Stern, Rev. Mod. Phys. **54**, 437 (1982).
[33] L. Resca and R. Resta, Phys. Rev. Lett. **44**, 1340 (1980).